Proceedings of the SEM Annual Conference
June 7-10, 2010 Indianapolis, Indiana USA

In-situ Optical Investigations of Hypervelocity Impact Induced Dynamic Fracture

Leslie E. Lamberson[1], Ares J. Rosakis
Graduate Aerospace Laboratories
California Institute of Technology
Pasadena, California 91125
Email: les@caltech.edu

Veronica Eliasson
Department of Mechanical & Aerospace Engineering
University of Southern California
Los Angeles, California 90089

ABSTRACT

Two independent optical methods are used to analyze the dynamic material behavior of Mylar and Homalite-100 subjected to hypervelocity impact. Birefringent targets are loaded in tension inside a two-stage light-gas gun vacuum chamber, and are impacted with a 5 mg nylon slug at velocities between 3 and 6 km/s. Caustics and photoelasticity combined with high-speed photography are used to determine dynamic stress intensity behavior around the crack tip during and after impact. Homalite-100 lower crack tip speeds are subjected to reflecting boundary shear waves from the nylon impact, and thereby the crack path exhibits distinct kinks; whereas Mylar higher crack tip speeds provides distinguishable isochromatic patterns and an unadulterated fracture surface. Shear wave patterns in the target from photoelastic effects are compared to results from numerical simulations using the Overture Suite, which solves linear elasticity equations on overlapping curvilinear grids by means of adaptive mesh refinement.

Introduction

Micrometeoroid and orbital debris (MMOD) damage from hypervelocity impact is a growing concern in space asset design. According to NASA Johnson's Orbital Debris Program Office there are currently over 7,000 pieces of tracked space debris in low Earth orbit (reaching up to 2 km above Earth's surface) over 1 cm in diameter and an estimated 50,000 pieces untracked of the same size [6]. Moreover, the International Space Station (ISS) currently has roughly 100 different types of MMOD shielding and still executes debris avoidance procedures [4]. While the size of the debris and micrometeoroids is relatively small, these impacts can induce strain rates up to $10^{-11}\mathrm{s}^{-1}$ and pressure rates in the Mbar range which can compromise the structural integrity as well as the optical, thermal or electrical functionality of a space vehicle. The threat of hypervelocity impact is real, yet little has been investigated involving the damage evolution resulting from these high-energy density events. This paper addresses the dynamic fracture behavior of brittle polymers subjected to hypervelocity impact.

While a generous amount of work has been done by NASA facilities investigating damage of various metals and composite materials from hypervelocity impacts, these studies mainly focus on generating equations to predict impact crater geometry [8]. What makes this study unique is that the dynamic fracture behavior of brittle polymers from this out-of-plane high-speed loading condition has never been rigorously investigated, yet brittle materials are often a critical component of space vehicles. For example, the James Webb Space Telescope scheduled to launch in 2013 has a tennis court sized sun-shield made of thin sheets of Kapton (a Mylar-like polymer) [1] and the newly finished Cupola on the ISS 'window to the world' is made from thick pieces of fused silica glass [5], while all windows on the current shuttle orbiter are a form of brittle

[1]Address all correspondence to this author.

T. Proulx (ed.), *Dynamic Behavior of Materials, Volume 1*, Conference Proceedings of the Society for Experimental Mechanics Series,
DOI 10.1007/978-1-4419-8228-5_6, © The Society for Experimental Mechanics, Inc. 2011

polymer. During hypervelocity impact, the incoming micrometeoroids and space debris are traveling at velocities at least 3 to over 10 times faster than the target material pressure wave speed, and as a result the inertial stresses outweigh the material strength in damage evolution.

The mechanics of a hypervelocity impact strike can be described from a fundamental perspective of a right-cylinder (length equal to diameter) impacting a semi-infinite plate of the same thickness as the projectile at a normal angle of incidence with hypervelocity speed. Upon contact, a shock wave travels to the rear of the projectile as well as to the rear of the target plate. At almost the same instant, rarefaction waves are generated on the boundary of impactor due to its much smaller size than the plate and propagate towards its axis of symmetry. A short time later the shock waves reach the rear surface of the plate and the projectile and reflect back as rarefaction waves to satisfy the stress free boundary conditions. The rarefaction waves can be thought of a tensile waves in the sense that if they are greater than the fracture strength of the material, the material will fracture (often as spall) in either the target or projectile material. When this occurs a new free surface is generated and a new rarefaction wave is created to satisfy the boundary conditions on the freshly created boundary. If the new rarefaction wave is greater than the fracture strength another fracture will occur, creating new spall and further damage. Consequently, the fracture process of hypervelocity impact can be described as a multiple spallation process initiated at fracture surfaces. Additionally, the initial shocking process is nonisentropic and rarefactions are isentropic. This mismatch in entropy generates energy often in the form of heat which contributes to the melting, vaporization and plasma formation at the strike site [3].

Experimental Configuration

Hypervelocity impacts were generated in the laboratory utilizing a two-stage light-gas gun jointly owned between NASA's Jet Propulsion Laboratory and the California Institute of Technology called the Small Particle Hypervelocity Impact Range (SPHIR). The two-stage light-gas gun creates micrometeoroid and orbital debris strikes initiating with a Sako 22-250 rifle action using 0.9 grams of smokeless gunpowder. This chemical ignition then sets in motion a small high-density polyethylene piston which compresses 150 psi of hydrogen in the pump-tube generating a high energy shock wave in stage one. From there, the gas is further accelerated in a small converging shape nozzle called the area-reservoir (AR) section where the piston gets extruded and stopped. On the downrange side of the AR section, a 5 mil thick film of Mylar is burst creating a uniform shock wave release on the launch package housed in the launch tube in stage two. In this case, launch packages are all nylon 6/6 right cylindrical slugs 5 mg with a length and diameter of 1.8 mm. Impact speeds ranged from 3 to 6 km/s. The projectile then goes into free flight under 1 Torr vacuum for 4 meters until striking the polymer plate in the target chamber. Two brittle polymer plates were considered in this investigation, Mylar and Homalite-100, between 1 and 6 mm in thickness and 150 mm in diameter. The plates were given notches and in some cases small pre-cracks (1-3 mm in length) and held in nominal tensile loads between 0.5 and 4 MPa on a load frame housed inside the target tank. These small loads helped to instigate mode-I crack growth (opening crack mode) and could serve as simulated membrane stresses of an external tank or cooling pipe or functional load on a working component of a space asset. A photograph of the SPHIR laboratory as well as a schematic of the optical diagnostics configuration is shown in Figures (1,2).

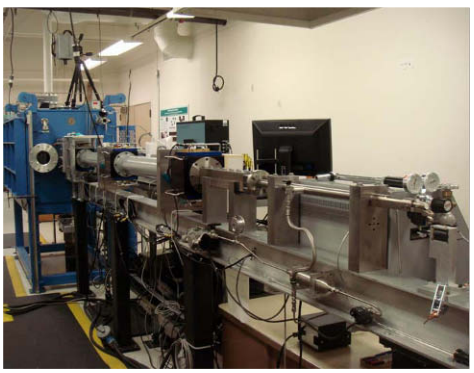

Figure 1: Photograph of SPHIR Laboratory.

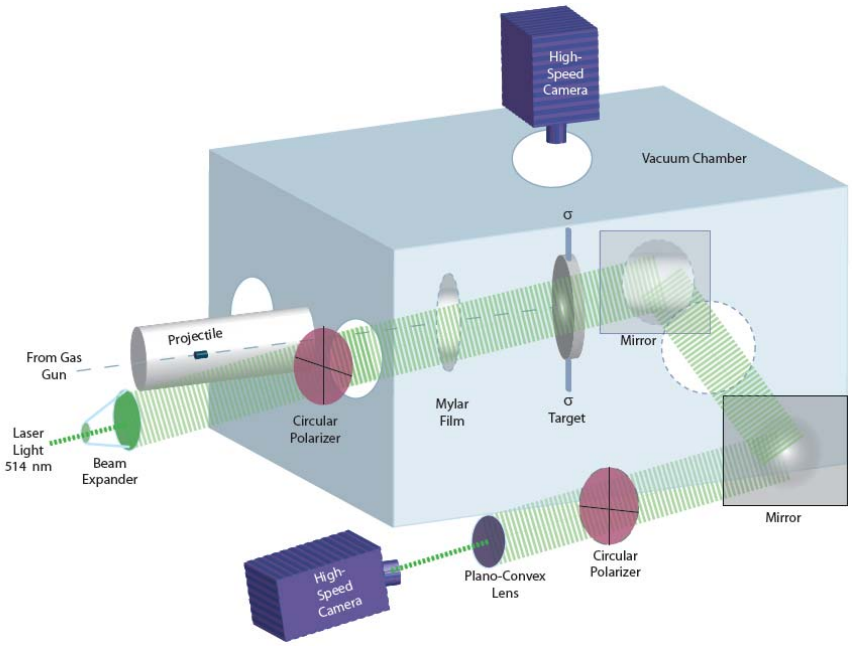

Figure 2: Schematic of optical diagnostics and high-speed photography configuration.

Method of Caustics

All optical analysis was performed in transmission. A monochromatic light source from an Argon-Ion laser was expanded to 100 mm diameter and fed into the target chamber of the two-stage light-gas gun, illuminating the target. A CORDIN 214-8 camera capable of capturing 8 frames at up to 100 million frames per second was set to focus on a virtual object plane at a distance z_0 behind the specimen. Due to the localized thinning at the crack tip, the incident light is refracted away generating a characteristic shadow spot near the region of the crack tip due to the displaced imaging plane [10]. While a circular polariscope was used to qualitatively investigate isochromatic patterns near the crack tip, caustics was used to quantitatively determine the energy ahead of the moving crack tip via the dynamic stress intensity factor. An example schematic of the caustics configuration is shown in Figure (3).

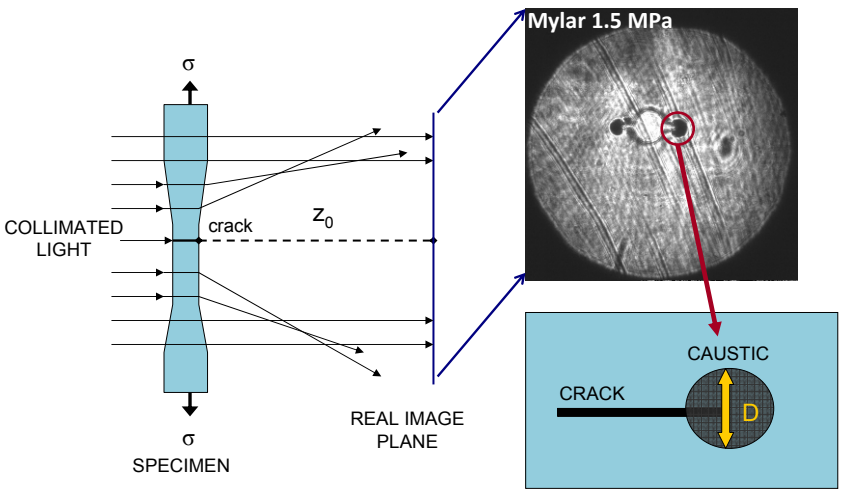

Figure 3: Schematic of method of caustics in transmission.

The method of caustics uses the dimensions of the shadow or caustic formed which dictates the value of the stress intensity factor at that instant in time. Assuming the near-tip stress distribution is characterized by only the first term of the steady-state asmyptotic stress solution originally proposed by Griffith in steady-state expansion [7] and the initial curve is approximated by a circle, the equation expressing the relationship is as follows

$$K_I^{dyn} = \frac{2}{3}\frac{\sqrt{2\pi}}{z_0 C t}\left(\frac{D}{3.163}\right)^{5/2}\frac{4\beta_1\beta_2 - (1+\beta_2^2)^2}{(\beta_1^2-\beta_2^2)(1+\beta_2^2)} \tag{1}$$

where D is the transverse diameter of the caustic, C is the stress optic coefficient, t is plate thickness, z_0 is the distance between the screen and the specimen, and $\beta_1 = (1-\nu^2/c_1^2)$ and $\beta_2 = (1-\nu^2/c_2^2)$, ν being the crack speed and c_1 and c_2 being the dilatational and distortional wave speeds of the plate [2]. The 3.163 value is empirically determined for these materials assuming optical isotropy [11].

By using the method of caustics to determine K_I^{dyn} we are pre-supposing that the fracture behavior will remain K-I dominant at the crack tip even though it is instigated by an extreme out-of-plane dynamic loading event. Depending on the results, we can then determine both if our mode-I dominant fracture criterion is appropriate and if local symmetry typically assumed at the crack tip on more classical mixed-mode loading problems is a valid approach to characterizing this complex phenomenon [9].

Results

Crack velocities were averaged using a secant method. No statistically significant correlation was determined between the location of the hypervelocity impact and resulting crack tip speeds, nor with the incoming projectile velocity and the resulting crack tip speeds. Resulting dynamic stress intensity values nondimensionalized by the material equivalent static value is plotted versus the crack speed nondimensionalized by the material Rayleigh wave speed and shown in Figure (4). While crack speeds seemed to be slightly slower in Homalite-100, on average, this material also tended to exhibit more transient crack behavior ahead of the crack tip. The nature of the transient crack behavior could be seen both in the dynamically changing sizes of the caustics in time of Homalite-100 as well as the distinct jagged or kinking behavior exhibited in the microscopy of the resulting crack taken after the impact event.

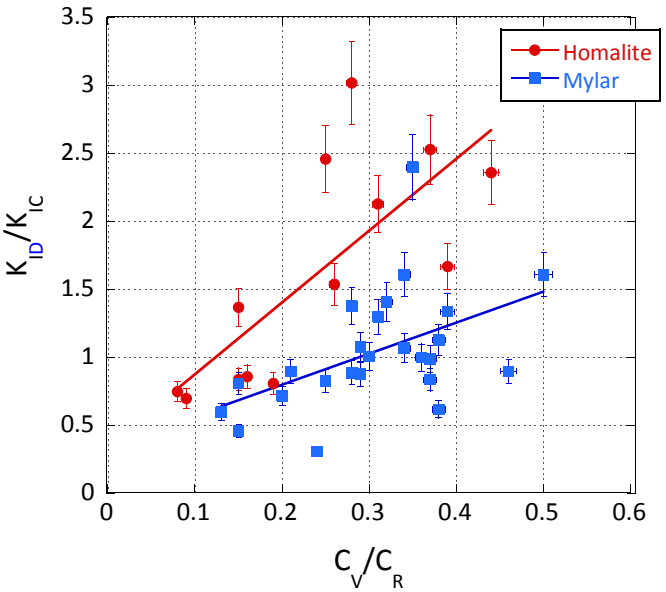

Figure 4: Plot of Mylar and Homalite-100 dynamic stress intensity factor normalized by static fracture toughness value versus the crack velocities normalized by the material Rayleigh wave speed.

Table 1: Summarized results of hypervelocity impact damage of brittle polymer investigation.

	Homalite-100	Mylar
P wave speed [m/s]	2145	2447
S wave speed [m/s]	1082	1185
Static Fracture Toughness [MPa/$\sqrt{m}$]	0.45	1.0
Averaged crack tip velocity [m/s]	230	330
Averaged Dynamic Stress Intensity [MPa/$\sqrt{m}$]	0.73	1.0
Crack path appearance	kinked	smooth

Generally, Mylar tended to transition from crack initiation to crack propagation sooner by approximately 20 ms than Homalite-100. Therefore, Mylar was able to completely fail before significant wave reflections and boundary interactions affected the moving crack. As a result, Mylar had a smooth and unadulterated crack path appearance and tended to follow directly behind the propagating shear wave from the impact site. Curiously, crack speeds remained relatively subsonic in nature, remaining between 0.2 to 0.5 the material Rayleigh wave speeds, yet there seemed to be an absence of extensive crazing ahead of the crack tip in Mylar. Branching was only seen when crack speeds reached its highest values in Homalite-100 and was not a common site along the crack path in post-analysis. Furthermore, Homalite-100 took longer to initiate cracking and as such had more complex wave action at the crack tip, most likely causing the crack path to continuously seek its local opening mode (or mode I crack growth) resulting in a kinked crack path appearance. Table (1) summarizes the results of the caustic investigation.

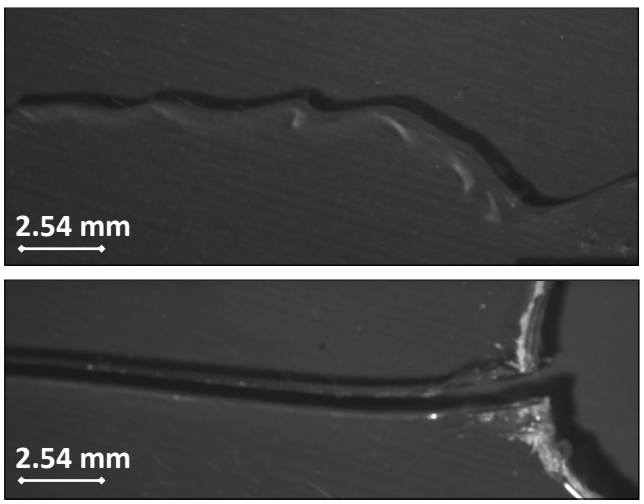

Figure 5: *(Top)* Homalite-100 microscopy image of kinked crack path appearance. *(Bottom)* Mylar microscopy image of smooth crack path appearance.

Overall the range of crack tip velocities and dynamic stress intensity values of both Mylar and Homalite-100 remained in a regime typically cited in literature under traditional in-plane lower loading rates to quasi-static loading rate behavior. The general noted trend of increasing dynamic stress intensity factor with increasing crack velocities can be seen. Error in the analysis predominantly came from the mismatch in the lack of temporal resolution in the full-field CORDIN images. Namely, the 8 images taken during the fracture initiated by the impact event had a 10 to 20 μs time scale, yet the behavior at the crack tip was dynamically changing on a time scale closer to 1 μs down to nanosecond scale. Additionally, the integrity of the measurement of the caustic could be questioned due to the multiple energetic phenomena happening in the region during impact including debris cloud and eject formation, vaporization of the projectile and melting. Despite of all the sources of error, the mixed-mode initiation loading conditions and the highly energetic interaction between the

projectile and the target, the predominant failure mode remained in-plane. This is most likely due to the fact that the slowest moving Rayleigh wave did not have time to propagate and interact with the boundaries enough to generate an out-of-plane bending moment before fracture completed. Therefore, in averaged sense, K_I or opening mode fracture criterion is relatively valid even in the complex event of a micrometeoroid and orbital debris strike.

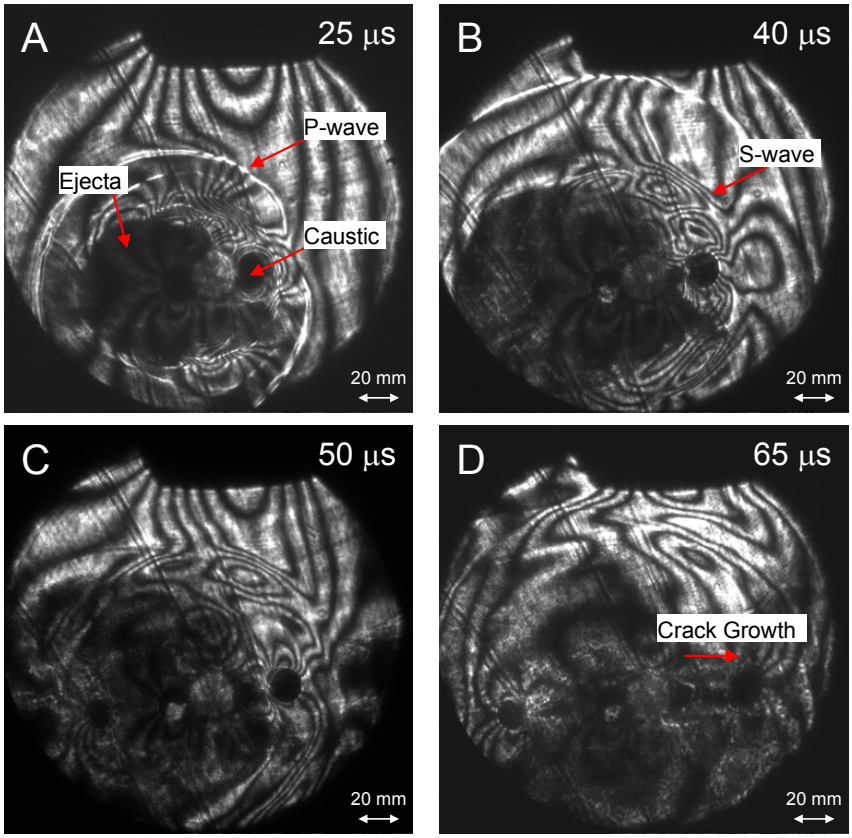

Figure 6: Caustics and isochromatic fringe patterns illustrating crack growth resulting from a hypervelocity impact strike on Mylar 1.6 mm thick at 5 km/s. (A) Shows initial P-wave radiating from impact site 25 μs after impact. Ejecta cloud at impact site can be seen. (B) Shows S-wave propagating soon after impact. Impact hole location and damage is clearly visible. (C),(D) Show noticeable crack growth via caustics as ejecta cloud disperses and stress wave patterns become more complex.

Next steps in this research include taking the results of the experimental fracture behavior of these brittle polymer plates under hypervelocity impacts and comparing them to numerical results from a 2-D in-plane code. In this case, initial endeavors in modeling the complex stress wave behavior from impact are being investigated using the Overture Suite, an adaptive mesh refinement finite difference method which solves the linear elasticity equations. Initial results indicate reasonable qualitative agreement in resulting wave pattern structure from computations and those captured with high-speed photography in the experiments. Future work will develop the code to output the difference in principle stress values in order to compare one-to-one with the isochromatic fringe patterns from the results at various times of interest during fracture. Lastly, future experimental investigations should probe conditions where, even in the averaged sense, the fracture criterion begins to fail by examining variables such as plate thickness (into plane strain regime), impact velocities, nominal tensile loads, initial crack sizes, and the like.

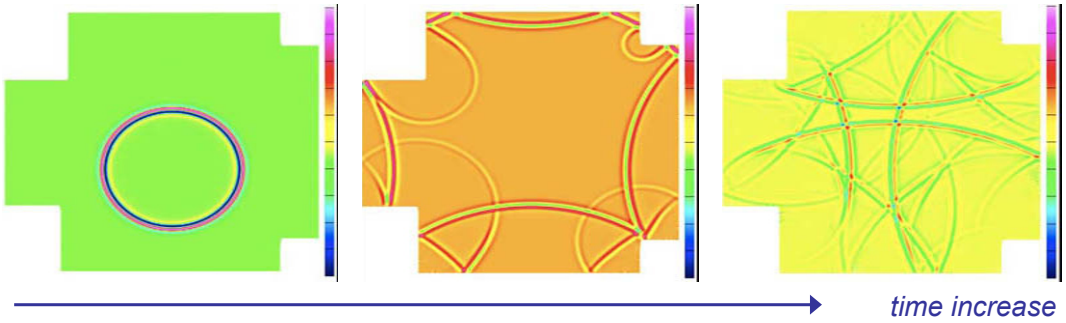

Figure 7: Example qualitative results from Overture of pressure wave patterns in Mylar from impact conditions as illustrated by color bar, which corresponds to the magnitude of the divergence. Left surface is clamped boundary condition, all others are free.

The authors acknowledge support from the Department of Energy Award DE-PS52-07NA28208 through the National Nuclear Security Administration, National Science Foundation Graduate Research Fellowship, as well as the NASA Aeronautics Scholarship Program through the American Society of Engineering Education.

References

[1] Jeanna Bryner. Huge sun shield built for space telescope. *SPACE*, December 2008.

[2] K. Ravi-Chandar C. Taudou. Experimental determination of the dynamic stress-intensity factor using caustics and photoelasticity. *Experimental Mechanics*, 32(3):203–210, 1992.

[3] A.R McMillan C.J. Maiden. An investigation of the protection afforded a spacecraft by a thin shield. *AIAA Journal*, 2(11):1992–1998, 1964.

[4] Aeronautics Committee on International Space Station Meteoriod/Debris Risk Management, Commission on Engineering Space Engineering Board, and National Research Council Technical Systems. *Protecting the Space Station from Meteoroids and Orbital Debris*. National Academy Press, 1997.

[5] Marcia Cunn. International space station gets a bay window. *Sci-Tech Today*, February 2010.

[6] Jr. D. F. Portree J. P. Loftus. Orbital debris: A chronology. Technical Report TP-1999-208856, NASA, 1999.

[7] L.B. Freund. *Dynamic Fracture Mechanics*. Cambridge University Press, 1990.

[8] S. A. Hill. Determination of an empirical model for the prediction of penetration hole diameter in thin plates from hypervelocity impact. *International Journal of Impact Engineering*, 30:303–321, 2004.

[9] K. Ravi-Chandar. Dynamic fracture of nominally brittle materials. *International Journal of Fracture*, 90:83–102, 1998.

[10] R. J. Rosakis S. Krishnaswamy. On the extent of dominance of asymptotic elastodynamic crack-tip fields; part i: and experimental study using bifocal caustics. *Journal of Applied Mechanics*, 8:87–95, 1991.

[11] George C. Sih, editor. *Experimental evalution of stress concentration and intensity factors*. Mechanics of Fracture 7. Martinus Nijhoff Publishers, 1981.